Available online at www.sciencedirect.com
ScienceDirect
European Journal of Medicinal Chemistry 42 (2007) 477–486
EUROPEAN JOURNAL OF MEDICINAL CHEMISTRY
http://www.elsevier.com/locate/ejmech

Original article

3D-QSAR and molecular docking studies on benzothiazole derivatives as *Candida albicans* *N*-myristoyltransferase inhibitors

Chunquan Sheng, Jie Zhu, Wannian Zhang*, Min Zhang, Haitao Ji, Yunlong Song, Hui Xu, Jianzhong Yao, Zhenyuan Miao, Youjun Zhou, Jü Zhu, Jiaguo Lü

School of Pharmacy, Military Key Laboratory of Medicinal Chemistry, Second Military Medical University, 325 Guohe Road, Shanghai 200433, People's Republic of China

Received 19 January 2006; received in revised form 13 October 2006; accepted 7 November 2006
Available online 18 November 2006

Abstract

N-Myristoyltransferase has been a promising new target for the design of novel antifungal agents with new mode of action. Molecular docking and three-dimensional quantitative structure–activity relationship (3D-QSAR) methods, CoMFA and CoMSIA, were applied to a set of novel benzothiazole *Candida albicans* *N*-myristoyltransferase (CaNmt) inhibitors. The binding mode of the compounds at the active site of CaNmt was explored using flexible docking method and various hydrophobic and hydrogen-bonding interactions were observed between the benzothiazole inhibitors and the target enzyme. The best CoMFA and CoMSIA models had a cross-validated coefficient q^2 of 0.733 and 0.738, respectively, which showed high correlative and predictive abilities on both the test set and training set. The 3D contour maps of CoMFA and CoMSIA provided smooth and interpretable explanation of the structure–activity relationship for the compounds. The analysis of the 3D contour plots permitted interesting conclusions about the effects of different substituent groups at different position of the benzothiazole ring, which will guide the design of novel CaNmt inhibitors with higher activity.

Keywords: 3D-QSAR; Molecular docking; Benzothiazole; *N*-Myristoyltransferase inhibitors; Antifungal

1. Introduction

During the past two decades, the life threatening infections caused by pathogenic fungi are becoming increasingly common, especially in those individuals with immunocompromised hosts, such as patients undergoing anticancer chemotherapy or organ transplants and patients with AIDS [1]. Clinically, candidosis, aspergillosis and cryptococcosis are three major fungal infections in immunocompromised individuals [2,3]. The common antifungal agents currently used in clinic are azoles (such as fluconazole, ketoconazole and itraconazole), polyenes (such as amphotericin B and nystatin), echinocandins (such as caspofungin and micafungin) and allylamines (such as naftifine and terbinafine). However, their use can suffer from limited efficiency, narrow antifungal spectrum, drug related toxicity, severer drug resistance, non-optimal pharmacokinetics and serious drug–drug interactions. Therefore, there is an emergent need to develop novel fungicidal drugs with a new mode of action.

Myristoyl-CoA:protein *N*-myristoyltransferase (Nmt) is a cytosolic monomeric enzyme that catalyzes the transfer of the myristoyl group from myristoyl-CoA to the N-terminal glycine of a number of eukaryotic cellular and viral proteins [4,5]. Myristoylation relates to diverse biological processes including signal transduction cascades and apoptosis. Genetic experiments have shown that Nmt is an essential enzyme for the viability of some important pathogenic fungi including *Candida albicans* and *Cryptococcus neoformans* [6,7]. Thus, Nmt has been a promising target enzyme for the development of novel fungicidal drugs having a broad antifungal spectrum

* Corresponding author. Tel./fax: +86 21 25074460.
E-mail address: zhangwnk@hotmail.com (W. Zhang).

0223-5234/$ - see front matter © 2006 Elsevier Masson SAS. All rights reserved.
doi:10.1016/j.ejmech.2006.11.001

[8]. Although Nmt also exists in human, the differences in the protein substrate specificities of fungal and human Nmts have been utilized to develop species-selective inhibitors that are fungicidal and safe [8].

Up to now, peptidomimetic inhibitors [9–12], myristic acid analogues [13,14], *p*-toluenesulfonamide inhibitors [15], benzofuran inhibitors [16–19] and benzothiazole inhibitors [20] have been reported to be Nmt inhibitors. Among them, the benzofuran and benzothiazole inhibitors showed high selectivity over human Nmt and exhibited good antifungal activity. Benzofuran inhibitors have been well studied *in vivo* and *in vitro* [16-19]. The structure–activity relationship (SAR) of benzofuran inhibitors has been studied by three quantitative structure–activity relationship (3D-QSAR) methods [21,22]. The binding mode of the benzofuran inhibitors was further clarified by the determination of the crystal structure of *Candida albicans* Nmt (CaNmt) in complex with benzofuran inhibitors [23]. Benzothiazole derivatives are relatively new class of Nmt inhibitors and no molecular modeling studies have been reported until now.

Among the current 3D-QSAR methods, comparative molecular field analysis (CoMFA) [24] and comparative molecular similarity indices analysis (CoMSIA) [25] are widely used in drug design, because they allow rapid prediction of the biological activities of newly designed molecules. To gain further insight into the SAR of the benzothiazole Nmt inhibitors, binding mode of this series of compounds was clarified by molecular docking, and CoMFA and CoMSIA were further applied to build robust 3D-QSAR models on them. The results deduced from the present investigation provided the useful information for the structural requirements of the benzothiazole Nmt inhibitors and could guide the rational design of novel CaNmt inhibitors.

2. Materials and methods

2.1. General

The crystallographic coordinates of CaNmt in complex with benzofuran inhibitor [23] (0.32 Å resolution, $R_{cryst} = 0.284$) were obtained from the Brookheaven Protein Databank as entries 1IYL. In the crystal structure, there are four asymmetric units (molecules A to D) with the inhibitor bound to the A and C asymmetric unit. In the present study, asymmetric unit C was used in our following docking study. All calculations were performed with commercially available SYBYL6.9 [26] and InsightII 2000 [27] software packages. All calculations were performed on an Origin 300 Server.

2.1.1. Data set

A total of 44 benzothiazole compounds from the literature [20] were used as a data set in the following 3D-QSAR analysis (Fig. 1). The selection of training set and test set is based on structural diversity and frequency of distribution of biological data by doing principal component analysis. As a result, eight compounds were selected as a test set, which represented a range of inhibitory activity similar to that of a training set and was used to evaluate the predictive power of the resulting models. In order to reinforce the reliability of their 3D-QSAR models, four benzofuran Nmt inhibitors (compounds **45**–**48**) [19] were selected as real external compounds (Fig. 2) and were added into the test set. The biological activity of each compound was expressed as inhibitory concentrations (IC_{50}) against CaNmt and $-\log(IC_{50})$ was used for the 3D-QSAR analysis.

2.1.2. Docking analysis

In order to find a suitable docking method for the CaNmt system, DOCK 4.0.1 [28], FlexX [29] and InsightII/Affinity [30] were investigated to reproduce the position for the benzofuran inhibitor in the crystal structure 1IYL. For DOCK 4.01, a Connolly surface of each active site was generated using QCPE429 program. A flexible docking was performed starting with a selection and matching of an anchor atom within a maximum of 500 orientations, followed by growth of the ligand with 25 configurations per cycle. The final step included relaxation of 100 simplex minimizations to a convergence of 0.1 kcal/mol. For FlexX, all default parameters, as implemented in the 6.9 release of SYBYL [26], were used. Cscore calculations were performed for ranking, and all 30 poses were inspected. For Affinity, Monte Carlo docking protocol was used by default parameters. For the docking results from each method, the corresponding RMSD between the crystal and docked conformation was computed. The comparison of the docking results revealed that Affinity was the most powerful method. As a result, Affinity was selected to study the binding mode of benzothiazole inhibitor with CaNmt.

Compound **39**, the most active compound in the data set, was used to investigate the binding mode of the benzofuran inhibitors. First, compound **39** was manually docked into the active site of CaNmt on the basis of the binding mode of benzofuran inhibitors to construct the starting enzyme–inhibitor complex [23]. Then, the flexible ligand docking procedure in the Affinity module within InsightII was used to define the lowest energy position for the substrate using a Monte Carlo docking protocol. All the atoms within a defined radius (8 Å) of the inhibitor were allowed to move. The solvation grid supplied with the Affinity program was used. If the resulting substrate/enzyme system was within a predefined energy tolerance of the previous structure, the system was subjected to minimization. The resulting structure was accepted on the basis of energy check, which used the Metropolis criterion, and also a check of RMS distance of the new structure versus the structure found so far. The final conformation was obtained through a simulation annealing procedure from 500 K to 300 K, and then 5000 rounds of energy minimization were performed to reach a convergence, where the resulting interaction energy values were used to define a rank order.

2.1.3. Molecular modeling and alignment

In the 3D-QSAR studies, pharmacophoric conformation and alignment rule are two major critical steps to get meaningful results. Because the crystal structure of CaNmt in complex with benzothiazole inhibitors has not been reported, molecular

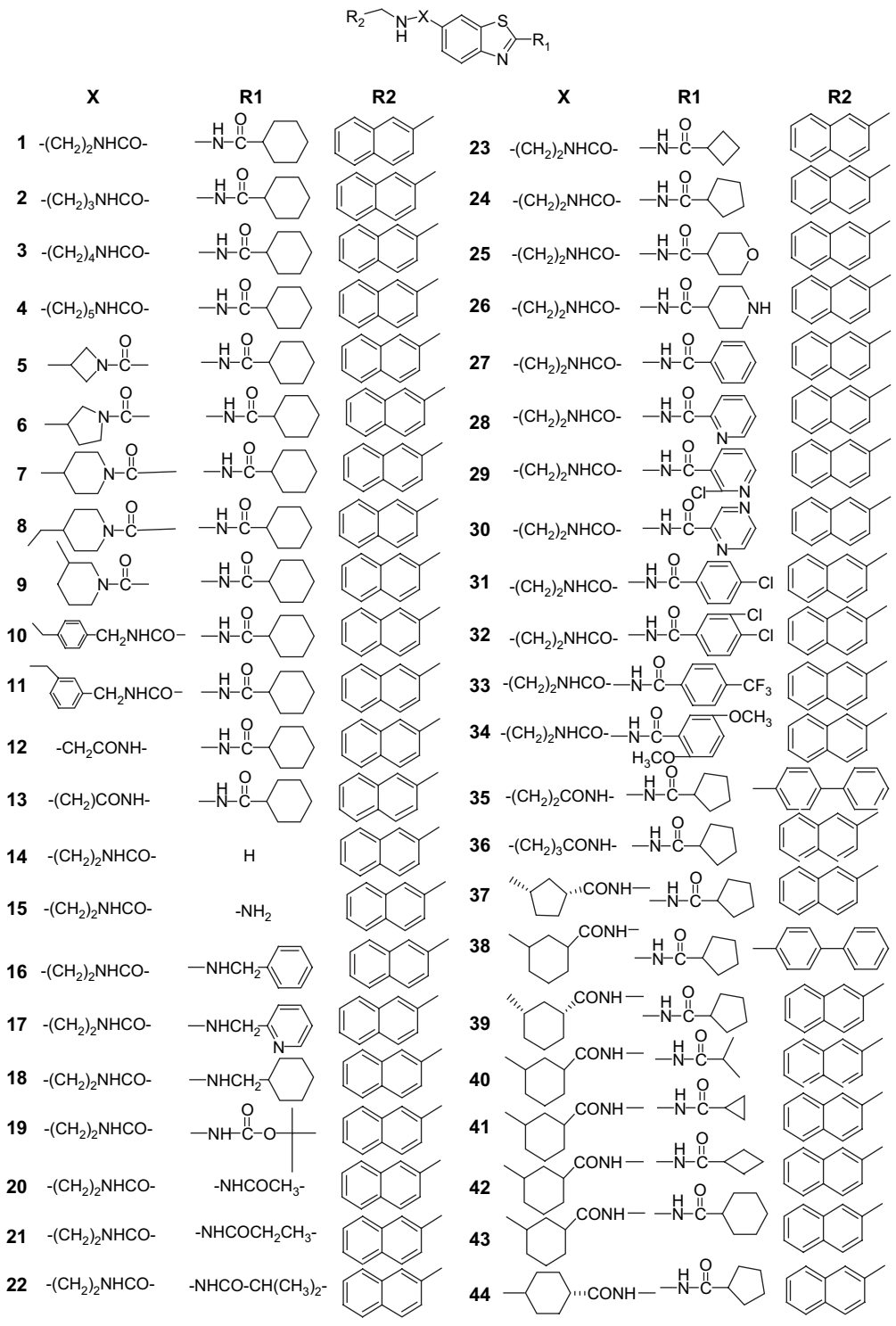

Fig. 1. Structures of the compounds in the training set and test set.

docking was used to simulate the pharmacophoric conformation. As a result, the docked conformation of compound **39** was used as the template to construct the structures of the remaining compounds in the data set. Energy minimization was performed using the Tripos force field, Powell optimization method, and MAXIMIN2 minimizer with a convergence criterion 0.001 Kcal/mol Å. Charges were calculated by the Gasteiger–Hückel method. Simulated annealing was then performed. The system was heated to 1000 K for 1.0 ps and then annealed to 250 K for 1.5 ps. The annealing function was exponential; 50 such cycles of annealing were run and the resulting 50 conformers were optimized using methods described above. The lowest energy conformation was selected. The alignment rule used in the present 3D-QSAR study was similar

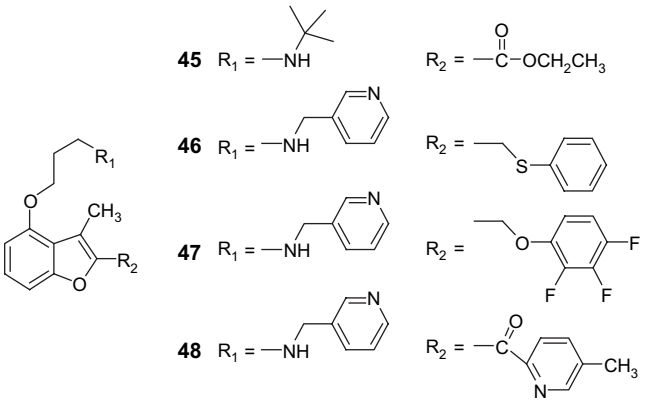

Fig. 2. Structures of the benzofuran Nmt inhibitors in the test set.

to that of the 3D-QSAR analysis on benzofuran inhibitors [31]. Compounds were aligned by RMS fitting of the atoms to the most active compound, compound **39**, based on the heavy atoms in the benzothiazole ring (Fig. 3). The superimposing of all the compounds is shown in Fig. 4.

2.1.4. CoMFA and CoMSIA setup

In deriving the CoMFA and CoMSIA descriptor fields, a 3D cubic lattice with grid spacing of 2 Å and extending 4 Å units beyond the aligned molecules in all directions was created to encompass the aligned molecules. The charges were calculated using the MOPAC AM1 Hamiltonian semiempirical method [32]. The CoMFA descriptors, steric (Lennard–Jones 6-12 potential) and electrostatic (Coulombic potential) field energies, were calculated by the following parameters: an sp^3 carbon probe atom with +1 charge and a Van der Waals radius of 1.52 Å, and energy cutoff of 30 kcal/mol. CoMSIA similarity indices descriptors (steric, electrostatic, hydrophobic, hydrogen-bond donor, and hydrogen-bond acceptor fields), were calculated using a C1+ probe atom with a radius of 1.0 Å placed at various grid spacing from 1 Å to 3 Å. CoMSIA similarity indices (A_F) for a molecule j with atoms i at a grid point q are calculated by Eq. (1):

$$A^q_{F,K}(j) = -\sum \omega_{\text{probe}'k}\omega_{ik}\, e^{-\alpha r^2_{iq}} \quad (1)$$

where k represents the following physicochemical properties: steric, electrostatic, hydrophobic, hydrogen-bond donor, and hydrogen-bond acceptor. A Gaussian-type distance-dependence was used between the grid point q and each atom i of

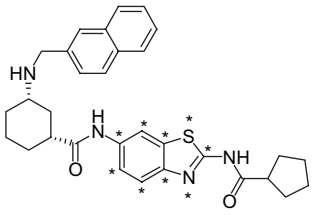

Fig. 3. Compound **39** as a template for superimposing by the heavy atoms of the benzothiazole ring (marked with asterisk).

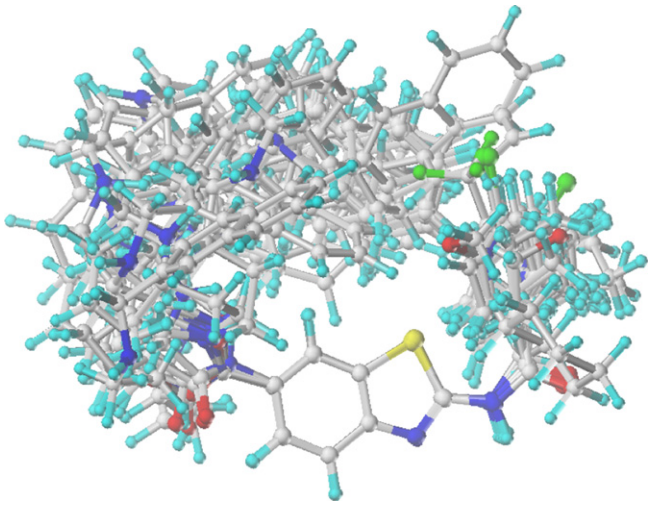

Fig. 4. Stereoview of the superimposed structures based on pharmacophoric conformation.

the molecule. Here, steric indices are related to the third power of the atomic radii, electrostatic descriptors are derived from atomic partial charges, hydrophobic fields are derived from atom-based parameters, and hydrogen-bond donor and acceptor indices are obtained by a rule-based method based on experimental results. The attenuation factor (α) was initially set to the default value of 0.3 and optimum values have been reported between 0.2 and 0.4, which was tested in the present study.

The CoMFA and CoMSIA descriptors were used as independent variables, and $p\text{IC}_{50}$ values were used as dependent variables in partial least squares (PLSs) regression analyses to derive 3D-QSAR models using the standard implementation in the SYBYL package. To obtain the optimal number of principle components, the leave-one-out (LOO) cross-validation was utilized, which is used to be a measure of how good the model represents the data in the training set. The cross-validated coefficient, q^2, was calculated using Eq. (2):

$$q^2 = 1 - \frac{\sum (Y_{\text{predicted}} - Y_{\text{observed}})^2}{\sum (Y_{\text{observed}} - Y_{\text{mean}})^2} \quad (2)$$

where $Y_{\text{predicted}}$, Y_{observed}, and Y_{mean} are predicted, observed, and mean values of the target property ($p\text{IC}_{50}$), respectively. To maintain the optimum number of PLS components and minimize the tendency to overfit the data, the number of components corresponding to the lowest PRESS value was used to derive the final PLS regression models. Conventional correlation coefficient r^2 and its standard error (s) were also computed for the final PLS models. To graphically interpret the 3D-QSAR results in terms of field contributions, isocontour maps were generated using the field type "stdev*coeff" and the contour levels were set to default values.

3. Results and discussion

3.1. Binding mode of the benzothiazole inhibitors

Our main goal for studies using the 1IYL model was to reproduce the position for benzofuran inhibitor seen in the crystal structure and verify our methodology. In the present studies, DOCK 4.0.1, FlexX and InsightII/Affinity were considered to evaluate their effectiveness. The RMSD between the docking conformation and the crystal conformation for the three docking methods are 2.114 Å, 2.015 Å and 1.259 Å, respectively. Moreover, the binding conformation of the benzofuran inhibitor derived from different docking methods was visual inspected. The binding conformation derived from Affinity was very similar to that in the crystal structure and important hydrogen-bonding interactions were retained. However, for another two docking method, important hydrogen-bonding interaction between Leu451 and amino group of C4-side chain was lost. Because the inhibitor recognition and binding is a process of ''induced-fit'', the conformation of both target enzyme and inhibitor would be changed during the enzyme–inhibitor interaction. The flexibility of both the active site of the target enzyme and the inhibitor is taken into account in the Affinity method, while only the flexibility of the inhibitor is considered in the other two docking methods. Because the Affinity method can obtain the best results, Affinity should be used as a powerful tool to clarify the binding mode of the benzothiazole inhibitors.

The binding mode of the compound **39** with the active site of CaNmt is shown in Fig. 5. The overall conformation of compound **39** in the active site was similar to that of the benzofuran inhibitors. The benzothiazole ring was located at the center of the active site, surrounded by some hydrophobic residues, such as Val108, Tyr225 and Leu451. Since the amide group of C2-side chain was important for the activity, the hydrogen-bonding interaction of the carbonyl O atom with the backbone amino group of Asp112, and the amide amino group with the side chain carboxyl group of Asp110 was observed. The cyclopentyl group attached to the amide group of C2-side chain was located into the strong hydrophobic region lined with Phe115, Phe240 and Phe339. It has been confirmed that Leu451 is an important functional residue in the catalytic cycle of CaNmt [23], and the docking results revealed that the second amine group of C6-side chain made a hydrogen bond with C-terminal carboxylate of Leu451, which was consistent with the binding mode of benzofuran inhibitors [23]. No direct interaction was observed between the amide group of C6-side chain and the active site of CaNmt. The cyclohexyl group between the amide and the secondary amine at C6-side chain could form hydrophobic interaction with Phe176 and Tyr107. Moreover, the cyclohexyl group could adjust the conformation of the C6-side chain, making the secondary amine group located a proper position to form hydrogen-bonding interaction with Leu451. A longer or more flexible group at this position would result in the decrease of the activity. The naphthyl group of C6-side chain was located into a narrow and hydrophobic pocket lined with Phe117, Leu337, Ile352, Tyr335 and Tyr354.

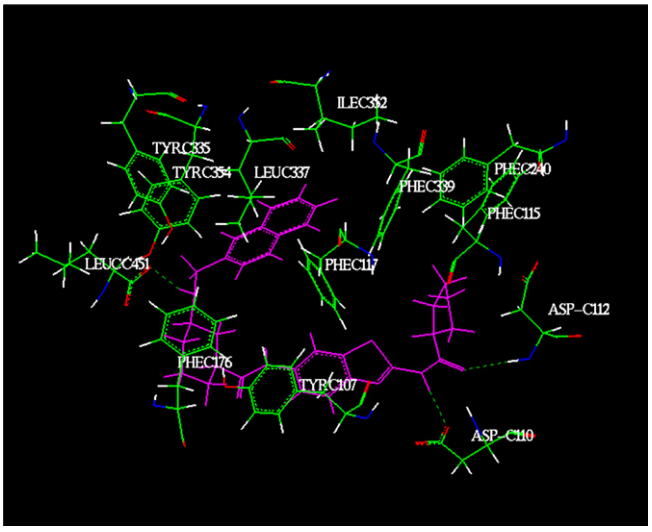

Fig. 5. Stereoview of the binding mode of compound **39** in the active site of CaNmt. The residues within 3 Å of the inhibitor are displayed and hydrogen bonds are displayed in dotted lines.

3.2. CoMFA and CoMSIA models

In an attempt to build robust 3D-QSAR models, variation of the parameters were considered during the 3D-QSAR studies. It has been discussed that the five different descriptor fields are not totally independent of each other and such dependencies of individual fields usually decrease the statistical significance of the models [33,34]. An evaluation, which of the five CoMSIA fields are actually needed for a predictive model, was performed by calculating all possible combinations of fields and the much faster SAMPLS [35] algorithm was used (Fig. 6). The first five models, using a single CoMSIA field, indicated that steric field and hydrophobic field were more important than the other three fields. The addition of hydrogen-bond donor field and hydrogen-bond acceptor field gave the best CoMSIA model ($q^2_{\mathrm{SAMPLS}} = 0.738$).

In CoMSIA calculation, the similarity indices are calculated using a Gaussian-type distance-dependence [25]. The attenuation factor α (see Eq. (1)) was initially set to the recommended value of 0.3 [25]. Larger α values result in a stronger attenuation of the distance-dependence of similarity considerations and therefore local features become more important over global molecular similarity, while smaller ones favor more global structure elements by a higher averaging of local features. Hence, the optimum α value is highly dependent on the actual problem, and we calculated q^2_{SAMPLS} for $0.1 < \alpha < 0.4$ in steps of 0.05. In this case, however, only decreased q^2_{SAMPLS} values for both higher and lower values of α were obtained (Table 1).

A correlation coefficient of r^2 of 0.987 and 0.978 and a cross-validated coefficient of q^2 of 0.733 and 0.738 were

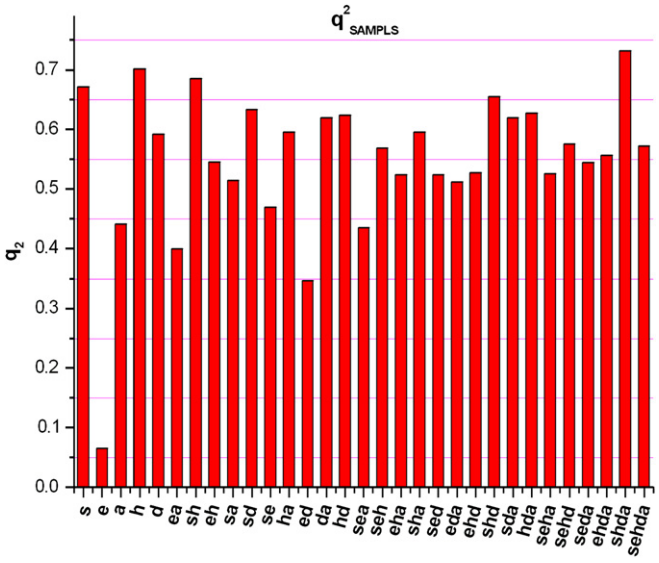

Fig. 6. Results of 31 possible CoMSIA field combinations (s = steric, e = electrostatic, h = hydrophobic, d/a = hydrogen-bond donor/acceptor) using q^2_{SAMPLS}.

obtained for the best CoMFA and CoMSIA model, respectively. The final CoMFA and CoMSIA model were satisfactory from the viewpoint of the statistical significance (see Table 2). The predictive ability of the training set and test set were evaluated, which indicated that the predictive IC_{50} values of the compounds correlated well with the experimental values (see Table 3, Figs. 7 and 8).

3.3. CoMFA and CoMSIA contour maps

To visualize the information content of the derived 3D-QSAR models, CoMFA and CoMSIA contour maps were generated. The field energies at each lattice point were calculated as the scalar results of the coefficient and the standard deviation associated with a particular column of the data table (''stdev*coeff''), which was always plotted as the percentage of the contribution to the CoMFA or CoMSIA equation.

Because CoMFA and CoMSIA contour map of steric field revealed similar results, only CoMFA contour map was shown.

Table 1
Influence of attenuation factor (α) on the CoMSIA models

	Model 1	Model 2	Model 3	Model 4	Model 5
α	0.2	0.25	0.3	0.35	0.4
q^2	0.591	0.614	0.738	0.656	0.664
r^2	0.934	0.953	0.978	0.961	0.979
Standard error	0.325	0.310	0.221	0.263	0.246
F	77.291	56.844	109.126	74.817	88.665
n	3	3	8	4	4
Fraction					
Steric	0.234	0.250	0.263	0.270	0.283
Hydrophobic	0.325	0.348	0.362	0.366	0.320
H-bond acceptor	0.198	0.184	0.174	0.168	0.165
H-bond donor	0.243	0.218	0.201	0.196	0.180

In Fig. 9a, the CoMFA contour map of steric field is displayed. The green contours represent the regions of high steric tolerance, while yellow contours represent regions of unfavorable steric effects (For interpretation of the references to colours in text, the reader is referred to the web version of this article.). The sterically disfavored regions were around the amide group of C6-side chain on the benzothiazole ring and also around the lateral part of naphthyl group, which indicates that compounds with larger substitutions are unfavorable for high inhibitory activity, e.g., the cyclization of the amide NH of C6-substituent on the benzothiazole ring of compounds **1**, **2**, and **3** with the alkyl part obtained the compounds with bulkier groups (compounds **5**, **6** and **7**), which led to the decrease of the inhibitory activity. The yellow region around the lateral part of naphthyl group can be well explained according to the SAR of the compounds. First, the length of C6-side chain was restricted. For example, if the substituent between 2-naphthyl and amide group was longer than 4 carbon–carbon bonds (such as in compounds **4**, **10** and **11**), the inhibitory activity would be decreased. Second, the substitution of 2-naphthyl with more bulkier biphenyl group (compound **38**) could lead to the decrease of the inhibitory activity. The sterically favored green regions were around the substituents on amide group of C2-side chain on the benzothiazole ring and also around the central part of naphthyl group. For example, the substituents on amide group of C2-side chain of compounds **20**, **21**, **22**, **23** and **24** are methyl, ethyl, isopropyl, cyclobutyl and cyclopentyl, respectively, and the bulkier substitutions leads to more active compounds. The green region on the central part of the naphthyl and the yellow region on the lateral part of the naphthyl indicated that the naphthyl group was important for the activity. Docking results have revealed that the naphthyl group was located into a narrow and hydrophobic pocket and bulkier or smaller groups are unfavorable for the interaction with the active site of CaNmt.

From the CoMFA model, the distribution of electrostatic field (0.267) was lower than that of steric field (0.733). Negatively charged (electron-rich) favorable red regions were found around the N and O atom of the amide group of C2-side chain on the benzothiazole ring and the N atom of the amide group of C6-side chain (Fig. 9b). These regions support the observation that the amide group of C2-side chain was important for the activity. If this amide group was substituted by the $-NH_2CH_2-$ (compound **18**), the inhibitory activity was decreased to a large extent. The red region around the N atom of the amide group of C6-side chain can be explained according to the SAR of compounds **5**, **6**, **7** and **9**. The negative charge on amide N atom was reduced by the cyclization of amide NH, which resulted in the decrease of the activity. The blue regions around the amide O atom of C6-side chain and the substituents on the amide group of C2-side chain represent an area where positive charge is favored (Fig. 9b). This result is in good agreement with the fact that compounds with the reversed amide of C6-side chain are among the compounds with the highest inhibitory activity. Also, the large blue region around the substituents on the amide group of C2-side chain can be explained by the fact that the activity of compounds

Table 2
The statistical parameters for the final CoMFA and CoMSIA model

	q^2	r^2	Standard error	F	n	Fraction				
						S	E	H	A	D
CoMFA	0.733	0.987	0.204	116.923	5	0.733	0.267			
CoMSIA	0.738	0.978	0.221	109.126	8	0.263		0.362	0.174	0.201

Table 3
Comparison of experimentally observed and CoMFA, CoMSIA predicted activities (pIC$_{50}$ and IC$_{50}$) for the training set and test set

Compound	IC$_{50}$ (μM)	pIC$_{50}$	CoMFA calcd. pIC$_{50}$	CoMFA calcd. IC$_{50}$ (μM)	CoMSIA calcd. pIC$_{50}$	CoMSIA calcd. IC$_{50}$ (μM)
Training set						
2	0.11	0.959	0.845	0.143	1.149	0.071
3	0.074	1.131	0.694	0.202	1.153	0.070
4	0.3	0.523	0.558	0.277	0.504	0.313
5	0.065	1.187	0.978	0.105	1.156	0.070
6	0.19	0.721	0.774	0.168	0.653	0.222
7	0.5	0.301	0.250	0.562	0.335	0.462
8	0.026	1.585	1.581	0.026	1.461	0.035
9	0.21	0.678	0.788	0.163	0.685	0.207
10	>10	−1.000	−0.854	7.145	−0.980	9.550
11	1.9	−0.279	−0.274	1.879	−0.160	1.445
12	2.3	−0.362	−0.189	1.545	−0.444	2.780
13	0.18	0.745	0.843	0.144	0.747	0.179
14	>10	−1.000	−1.110	12.882	−1.038	10.914
15	>10	−1.000	−1.008	10.186	−1.007	10.162
16	>10	−1.000	−0.939	8.690	−1.130	13.490
17	>10	−1.000	−0.931	8.531	−1.038	10.914
18	>1	0.000	0.070	0.851	0.120	0.759
20	>10	−1.000	−0.300	1.995	−0.360	2.291
21	0.13	0.886	0.201	0.630	0.396	0.402
22	0.046	1.337	1.454	0.035	1.477	0.033
24	0.023	1.638	1.089	0.081	1.567	0.027
25	0.89	0.051	0.745	0.180	−0.067	1.167
28	>10	−1.000	−1.058	11.429	−0.876	7.516
29	>10	−1.000	−0.584	3.837	−0.898	7.907
31	>10	−1.000	−1.166	14.655	−1.105	12.735
32	>10	−1.000	−1.012	10.280	−1.006	10.139
33	>10	−1.000	−1.239	17.338	−1.061	11.508
34	0.31	0.509	0.254	0.557	0.542	0.287
35	0.16	0.796	0.946	0.113	0.793	0.161
36	0.015	1.824	1.758	0.017	1.654	0.022
37	0.011	1.959	1.915	0.012	1.853	0.014
39	0.00049	3.310	2.999	0.001	3.173	0.001
40	0.0033	2.482	2.679	0.002	2.624	0.002
41	0.0024	2.620	2.339	0.005	2.112	0.008
42	0.0023	2.638	2.810	0.002	2.699	0.002
44	0.034	1.469	1.273	0.053	1.499	0.032
Test set						
1	0.034	1.469	1.518	0.030	1.363	0.043
19	>10	−1.000	−0.952	8.954	−0.931	8.531
23	0.028	1.553	1.417	0.038	1.650	0.022
26	>10	−1.000	−1.117	13.092	−0.939	8.690
27	0.16	0.796	0.856	0.139	0.719	0.191
30	0.73	0.137	0.069	0.853	0.186	0.652
38	0.13	0.886	1.005	0.099	1.103	0.079
43	0.0081	2.092	2.311	0.005	2.345	0.005
45	1.7	−0.230	−0.381	2.404	−0.186	1.535
46	0.62	0.208	0.411	0.388	0.106	0.783
47	0.0057	2.244	2.118	0.008	2.364	0.004
48	0.00039	3.409	3.204	0.001	3.300	0.001

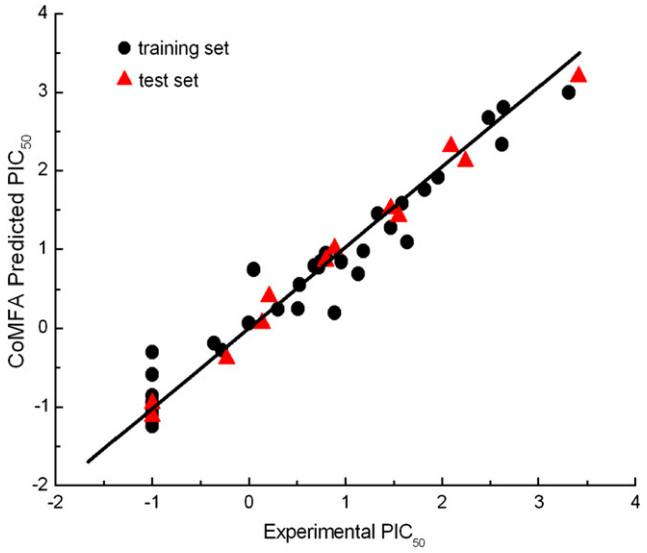

Fig. 7. Experimental and calculated pIC_{50} for the CoMFA analysis of the training set and test set.

31, **32** and **33** was lower than that of compound **27** because of the addition of electron-withdrawing group (such as Cl and CF_3) onto the phenyl group of compound **27**.

Furthermore, CoMSIA reveals three other contour maps that are not shown by CoMFA. Yellow regions in Fig. 10a indicate areas where hydrophobic substitutions are preferred and blue regions represent areas where hydrophobic substitutions are disfavored. The contour plot of hydrophobic field is similar to that of steric field. In fact, some steric large substituents are always hydrophobic. The hydrophobic favored regions are around the substituents on the amide group of C2-side chain, and the cyclohexyl and naphthyl group of C6-side chain. For example, when the cyclopropyl group on C2-side chain of compound **41** was replaced by more hydrophobic cyclobutyl

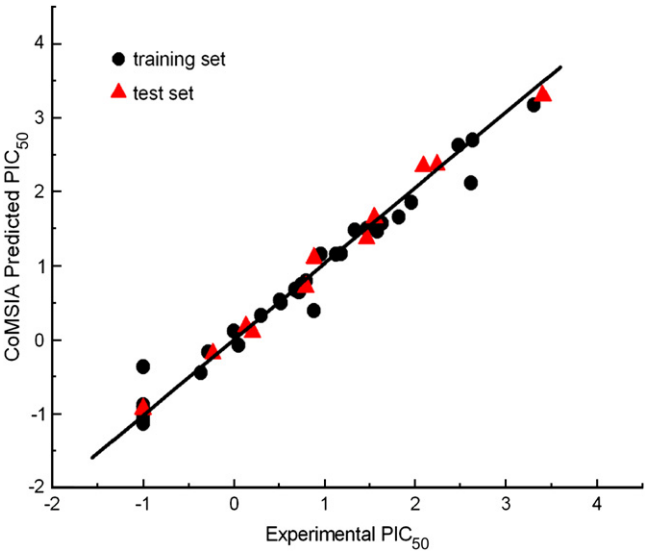

Fig. 8. Experimental and calculated pIC_{50} for the CoMSIA analysis of the training set and the test set.

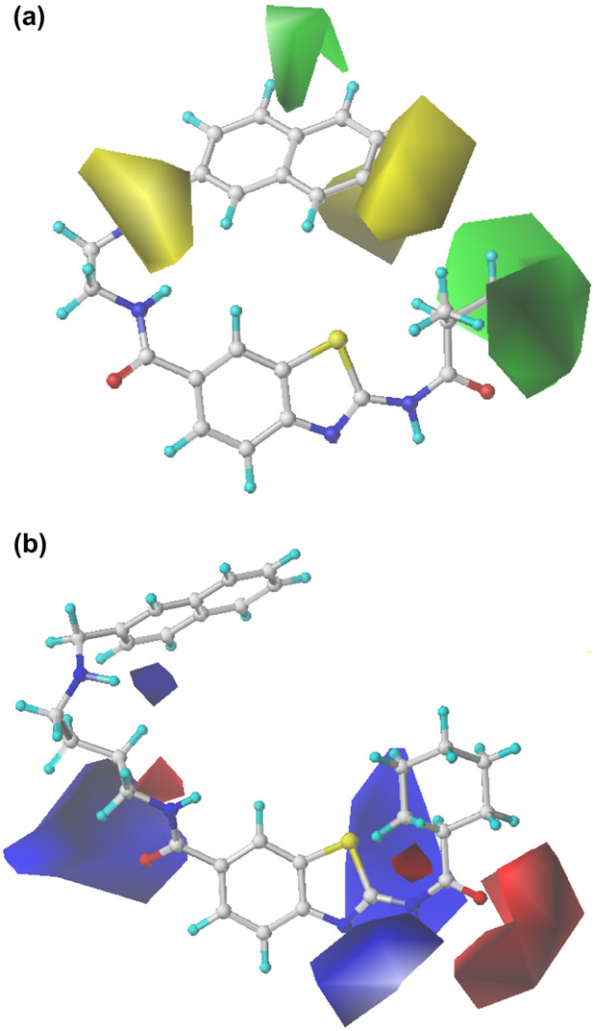

Fig. 9. The contour plots of CoMFA steric fields (a) and electrostatic fields (b).

and cyclopentyl groups (compounds **42** and **39**), the activity was accordingly increased. This result was in good agreement with the docking studies that the cyclopentyl group was located in the strong hydrophobic region lined with Phe115, Phe240 and Phe339. As shown in Fig. 10b and 10c, purple regions of hydrogen-bond acceptor field indicate that hydrogen-bond acceptor is favored and it is at the amide carbonyl group of the C2-side chain, while hydrogen-bond donor favored area in cyan is at the amide NH of C6-side chain and the secondary amine of C2-side chain. Thus, it is supposed that the amide group of C2-side chain and the secondary amine of C6-side chain could form hydrogen-bonding interaction with the active site of CaNmt, which is supported by the docking studies.

Analysis of CoMFA and CoMSIA contour plots revealed that the hydrogen-bond donor and acceptor groups and hydrophobic groups were necessary for the C2-side chain of benzothiazole ring. For the substitutions on the C6-side chain, secondary amine group with proper position was essential for the activity. Moreover, hydrophobic group with proper volume should be linked to the secondary amine at C6-side chain.

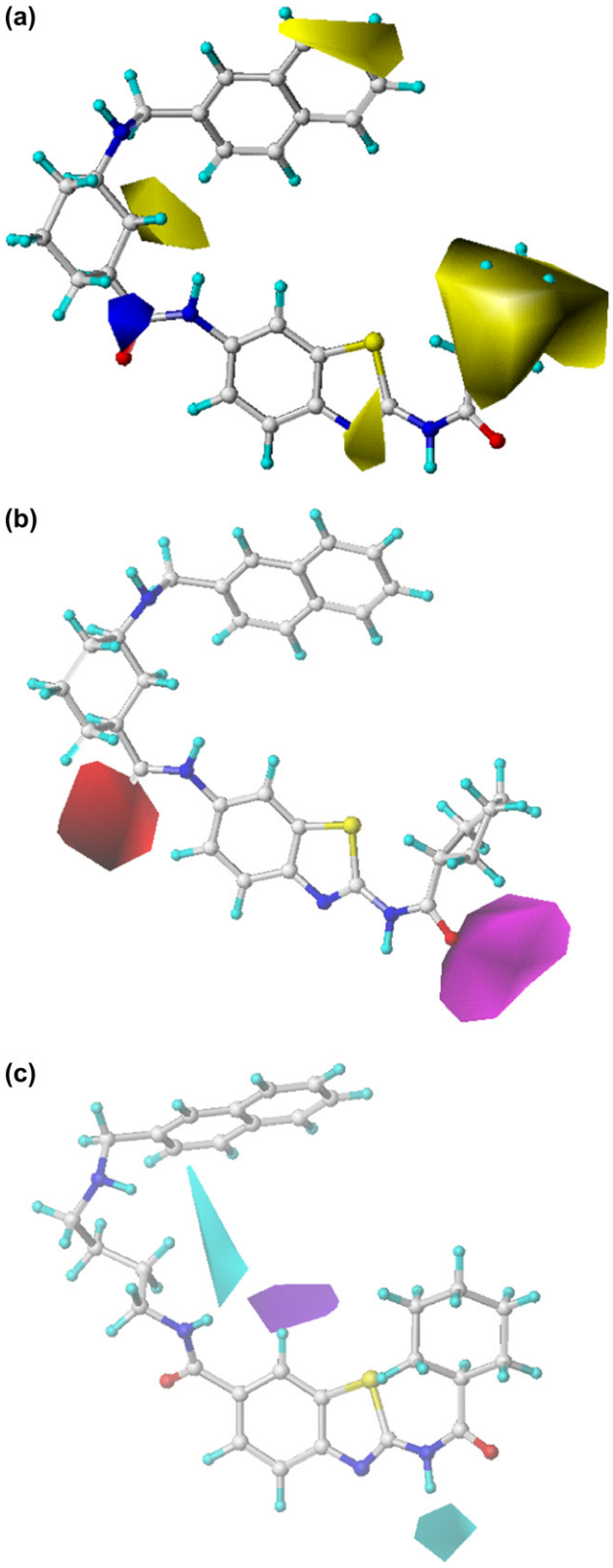

Fig. 10. The contour plots of CoMSIA hydrophobic fields (a), hydrogen-bond acceptor fields (b) and hydrogen-bond donor fields (c).

4. Conclusion

The emergent need for novel azole antifungal agents with new mode of action was a stimulus for the understanding of the structural features necessary for the Nmt inhibitors. In the present study, molecular docking and 3D-QSAR analysis has been successfully applied to a set of recently synthesized CaNmt inhibitors with benzothiazole scaffolds. The binding mode of the benzothiazole inhibitors was clarified by the flexible docking method and hydrogen-bonding interaction and hydrophobic interaction were found to be important for the inhibitor binding. Using the conformation generated from the docking study, highly predictive CoMFA and CoMSIA models were developed on benzothiazole inhibitors. The best derived CoMFA and CoMSIA model showed a predictive q^2 value of 0.733 and 0.738, and the activities of compounds in the training set and test set were predicted with good accuracy. Overall, the predictive power of the CoMSIA models appeared to be better than that of the CoMFA models. However, a combined application of the CoMFA and the CoMSIA models may be most suitable to predict the binding affinity of new CaNmt inhibitors. The 3D contour plots derived from 3D-QSAR studies provide many useful insights into relationships between structural features and inhibitory activity and also give a picture of the main chemical features crucial for the significant CaNmt inhibitory activity, which shows good correlation with the docking results. The combination of the results from molecular docking and 3D-QSAR analysis revealed that there are four important chemical elements which are essential for the inhibitory activity against CaNmt. Firstly, a hydrophobic aromatic core fragment should be located in the center of the active site of CaNmt; secondly, an amino group is required to form hydrogen-bonding interaction with the important functional residue Leu451; thirdly, two hydrophobic groups should be located in the two hydrophobic pockets in the active site and form hydrophobic interaction with them. Lastly, in order to improve the activity, additional hydrogen-bond acceptor or donor should be introduced into the molecule to interact with some important residues, such as Asp110 and Asp112. The above information can be used to design new lead compounds showing higher inhibitory activities and the chemical synthesis of new compounds is in progress.

Acknowledgement

This work was supported by the National Natural Science Foundation of China (Grant Nos. 30400567).

References

[1] S.K. Fridkin, W.R. Jarvis, Clin. Microbiol. Rev. 9 (1996) 499–511.
[2] J.P. Latge, Clin. Microbiol. Rev. 12 (1999) 310–350.
[3] J.N. Steenbergen, A.J. Casadevall, J. Clin. Microbiol. 38 (2000) 1974–1976.
[4] J.A. Boutin, Cell Signal. 9 (1997) 15–35.
[5] T.A. Farazi, G. Waksman, J.I. Gordon, J. Biol. Chem. 276 (2001) 39501–39504.

[6] J.K. Lodge, E. Jackson-Machelski, D.L. Toffaletti, Proc. Natl. Acad. Sci. U.S.A. 91 (1994) 12008–12012.
[7] H. Nakayama, T. Mio, S. Nagahashi, Infect. Immun. 68 (2000) 6712–6719.
[8] N.H. Georgopapadakou, Expert. Opin. Investig. Drugs 11 (2002) 1117–1125.
[9] B. Devadas, M.E. Zupec, S.K. Freeman, J. Med. Chem. 38 (1995) 1837–1840.
[10] S.R. Nagarajan, B. Devadas, M.E. Zupec, J. Med. Chem. 40 (1997) 1422–1438.
[11] B. Devadas, S.K. Freeman, M.E. Zupec, J. Med. Chem. 40 (1997) 2609–2625.
[12] B. Devadas, S.K. Freeman, C.A. McWherter, J. Med. Chem. 41 (1998) 996–1000.
[13] K. Parang, E.E. Knaus, L.I. Wiebe, Arch. Pharm. Pharm. Med. Chem. 329 (1996) 475–482.
[14] L.A. Paige, G. Zheng, S.A. DeFrees, Biochemistry 29 (1990) 10566–10573.
[15] R.G. Karki, V.M. Kulkarni, Indian Drugs 38 (2001) 406–408.
[16] M. Masubuchi, K. Kawasaki, H. Ebiike, Bioorg. Med. Chem. Lett. 11 (2001) 1833–1837.
[17] H. Ebiike, M. Masubuchi, P. Liu, Bioorg. Med. Chem. Lett. 12 (2002) 607–610.
[18] K. Kawasaki, M. Masubuchi, K. Morikami, Bioorg. Med. Chem. Lett. 13 (2003) 87–91.
[19] M. Masubuchi, H. Ebiike, K. Kawasaki, Bioorg. Med. Chem. 11 (2003) 4463–4478.
[20] K. Yamazaki, Y. Kaneko, K. Suwa, Bioorg. Med. Chem. 13 (2005) 2509–2522.
[21] P. Purushottamachar, V.M. Kulkarni, Bioorg. Med. Chem. 11 (2003) 3481–3497.
[22] K. Hasegawa, K. Morikami, Y. Shiratori, Chemometr. Intell. Lab. Syst. 69 (2003) 51–57.
[23] S. Sogabe, M. Masubuchi, K. Sakata, Chem. Biol. 9 (2002) 1119–1128.
[24] R.D. Cramer, D.E. Patterson, J.D. Bunce, J. Am. Chem. Soc. 110 (1988) 5959–5967.
[25] G. Klebe, U. Abraham, T. Mietzner, J. Med. Chem. 37 (1994) 4130–4146.
[26] SYBYL 6.9, Tripos Associates, Inc., 1699S, Hanley Road, Suite 303, St. Louis, MO 63144, 2003.
[27] InsightII 2000, Molecular Simulation Inc., 9685, Scranton Road, San Diego, CA 92121-3752, 1999.
[28] I.D. Kuntz, J.M. Blaney, S.J. Oatley, J. Mol. Biol. 161 (1982) 269–288.
[29] M. Rarey, B. Kramer, T. Lengauer, J. Mol. Biol. 261 (1996) 470–489.
[30] B.A. Luty, Z.R. Wasserman, P.F. Stouten, J. Comput. Chem. 16 (1995) 454–464.
[31] J. Zhu, C. Sheng, M. Zhang, Chem. J. Chin. Univ. 27 (2006) 287–291.
[32] M.J.S. Dewar, E.G. Zoebisch, E.F. Healy, J. Am. Chem. Soc. 107 (1985) 3902–3909.
[33] G. Bringmann, C.J. Rummey, J. Chem. Inf. Comput. Sci. 43 (2003) 304–316.
[34] M. Bohm, J. St rzebecher, G. Klebe, J. Med. Chem. 42 (1999) 458–477.
[35] B.L. Bush, R.B. Nachbar, J. Comput. Aided Mol. Des. 7 (1993) 587–619.